# Impact of edge magnetic perturbation (MP) on multi-scale turbulence and turbulent transport across a MP-induced edge transport reduction in the TEXTOR tokamak

Cite as: Phys. Plasmas **27**, 062511 (2020); https://doi.org/10.1063/5.0002022 Submitted: 23 January 2020 . Accepted: 19 May 2020 . Published Online: 15 June 2020

🧓 Y. He, Y. Xu, I. Shesterikov, M. Vergote, M. Van Schoor, A. Krämer-Flecken, and J. Cheng







### ARTICLES YOU MAY BE INTERESTED IN

Gyrokinetic understanding of the edge pedestal transport driven by resonant magnetic perturbations in a realistic divertor geometry

Physics of Plasmas 27, 062301 (2020); https://doi.org/10.1063/1.5144445

Role of sheared E × B flow in self-organized, improved confinement states in magnetized plasmas

Physics of Plasmas 27, 060501 (2020); https://doi.org/10.1063/1.5142734

Effect of magnetic perturbations on turbulence-flow dynamics at the L-H transition on DIII-D Physics of Plasmas 27, 062507 (2020); https://doi.org/10.1063/1.5145207





### Impact of edge magnetic perturbation (MP) on multi-scale turbulence and turbulent transport across a MP-induced edge transport reduction in the TEXTOR tokamak

Cite as: Phys. Plasmas **27**, 062511 (2020); doi: 10.1063/5.0002022 Submitted: 23 January 2020 · Accepted: 19 May 2020 ·

Published Online: 15 June 2020







Y. He, 1 🕞 Y. Xu, 1,a) I. Shesterikov, 2 M. Vergote, 2 M. Van Schoor, 2 A. Krämer-Flecken, 3 and J. Cheng

### **AFFILIATIONS**

- Institute of Fusion Science, School of Physical Science and Technology, Southwest Jiaotong University, Chengdu 610031, Sichuan, People's Republic of China
- <sup>2</sup>Laboratoire de Physique des Plasmas-Laboratorium voor Plasmafysica, Ecole Royale Militaire-Koninklijke Militaire School, Trilateral Euregio Cluster, B-1000 Brussels, Belgium
- <sup>3</sup>Institute of Energy and Climate Research-Plasma Physics, Forschungszentrum Jülich GmbH, Association EURATOM-FZJ, Trilateral Euregio Cluster, D-52425 Jülich, Germany

### **ABSTRACT**

Reduced particle losses have been observed during the operation of an m/n = 6/2 resonant magnetic perturbation in the TEXTOR tokamak. The influence of the perturbation field on multi-scale turbulence and turbulent transport has been surveyed in detail across the perturbation-induced reduction of edge transport. The results indicate that with magnetic perturbation (MP), both the large-scale zonal flows and small-scale drift-wave turbulence are significantly reduced. At high MP currents, a reduction of edge transport can be realized due to primarily the decline of small-scale ambient turbulence and turbulent transport in the ergodic zone, where the turbulence eddy size is largely decreased. Investigation on the dynamic process of fluctuation quantities during the perturbation current ramp-up phase further shows that geodesic acoustic mode zonal flows and their nonlinear interaction with background turbulence decrease incessantly with increasing perturbation current. The transport reduction takes place only after small-scale turbulence starts to be strongly reduced by the MP when the MP strength reaches a certain threshold value.

Published under license by AIP Publishing. https://doi.org/10.1063/5.0002022

### I. INTRODUCTION

In recent years, the application of resonant magnetic perturbation in magnetically confined plasmas has been demonstrated to be a promising way for suppression or mitigation of the edge localized mode<sup>1–4</sup> and control of MHD activities.<sup>5–7</sup> As the magnetic perturbation (MP) strongly modifies the magnetic topology at the plasma boundary, the influence of the perturbation field on the edge radial electric field, plasma rotations, turbulence, and turbulent transport, as well as zonal flows, has also been observed in many fusion devices.<sup>8–21</sup> For most RMP experiments performed in the H-mode regime, where the plasma stability and confinement depend crucially on the properties of the plasma pedestal, which is characterized by steep pressure and current gradients, the effects of the magnetic perturbation are commonly corroborated to be associated with the changes in edge magnetic topology and potential responses of instabilities in a specific phase-space

operating window of the 3D field. In contrast, the present study is based on Ohmic experiments, for which the influence of the magnetic perturbation on plasma properties reflects more on the change in fundamental features of edge turbulence and associated transport in the stochastic region induced by the MP. In an earlier paper, an improved confinement scenario during a static m/n = 6/2 MP operation at TEXTOR has been reported.<sup>22</sup> The substantial particle confinement is thought to be related to a particular condition in which edge magnetic flux tubes are connected to the wall, and the density built up is tentatively attributed to the modification of the electric potential induced by the open field lines with the MP. Nevertheless, a detailed investigation on the underlying physical mechanisms responsible for the confinement improvement or transport reduction, especially the influence of the MP on turbulence and associated transport, has not yet been carried out due to the lack of related diagnostics in the experimental campaign.

a) Author to whom correspondence should be addressed: xuyuhong@swjtu.edu.cn

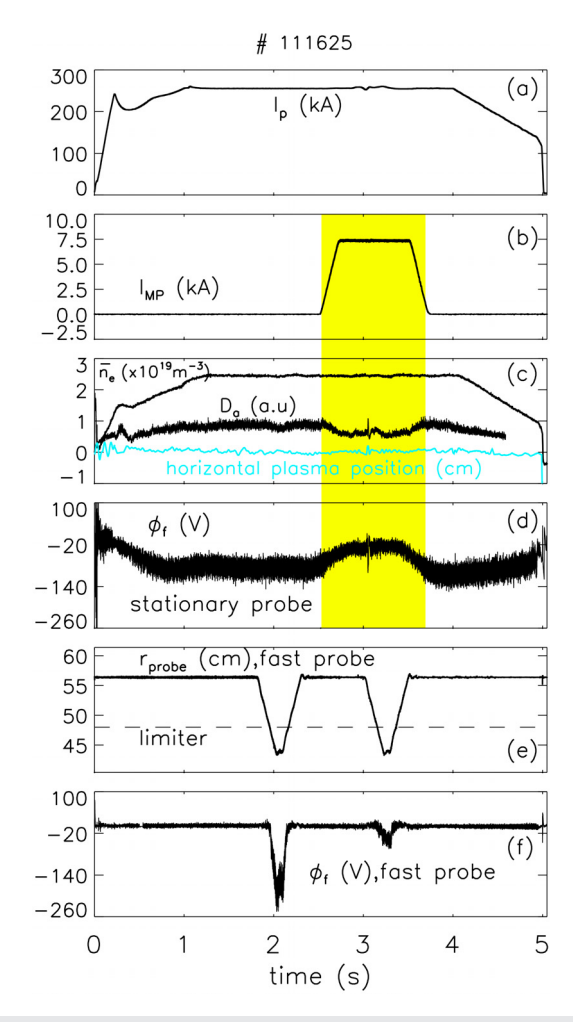
In this study, we have revisited the experimental scenario performed several years ago at the TEXTOR tokamak where a peculiar improved Ohmic confinement regime with reduced particle losses was reached in the static m/n = 6/2 DED experiment. The main purpose of this work is to investigate the impact of the edge magnetic perturbation on multi-scale turbulence, including micro-scale turbulence and meso-scale zonal flows, as well as turbulence-driven transport in such a scenario, in order to gain insight into multi-scale turbulence dynamics in the case of perturbed edge magnetic topology. The results provide new experimental evidence for the impact of the MP to induce a reduced edge turbulent transport in the stochastic region of ohmically heated plasmas and also the dynamic interaction between the zonal flows and microturbulence along with the threshold MP current to affect the particle confinement during the ramp-up of the MP current. The rest of this paper is organized as follows: In Sec. II, the experimental setup and diagnostics are described. Section III presents experimental results and discussions, and conclusions are formulated in Sec. IV.

### II. EXPERIMENTAL SETUP

The experiments were carried out in Ohmic deuterium discharges at TEXTOR with a limiter configuration. The major and minor radii are R = 175 cm and  $a \approx 48$  cm, respectively. The plasma current was  $I_p = (200-250)$  kA, the toroidal magnetic field was  $B_T$  = (1.9-2.25) T, and the central chord-averaged density was  $\bar{n}_e = (2.0-3.0) \times 10^{19} \text{ m}^{-3}$ . The edge resonant magnetic perturbation was generated by 16 coils, helically wound around the inner side of the torus with a pitch angle parallel to field lines on the rational magnetic surface with a safety factor  $q \approx 3.^{23}$  In the present experiment, the base poloidal/toroidal modes were operated as m/n = 6/2 with a dc current in the MP coils, which were applied during the stationary phase of the Ohmic discharge. The magnitude of the MP current,  $I_{MP}$ , was scanned in a range of  $I_{MP}$  = (3-7.5) kA. The main diagnostics used in this study were two sets of movable Langmuir probe systems installed on the outer midplane (low-field side) at two toroidally opposite locations of the torus. In each shot, one probe system is stationary, while the other is fast reciprocating. From shot to shot, the radial position of the stationary probe can be altered from the scrape-off layer (SOL) to the plasma edge. For the fast probe system, its head consists of two probe arrays separated by 4 mm in the radial direction.<sup>24</sup> The cylindrical molybdenum tips in both arrays of the fast probe are 3 mm long with a diameter of 1-2 mm. One probe array was connected as a "triple probe"  $^{25}$  to measure the local electron temperature  $T_e$ , density  $n_e$ , floating potential  $\phi_f$ , and plasma potential  $\phi_p = \phi_f + 2.8T_e$  in deuterium plasmas, <sup>26</sup> as well as fluctuation-induced particle flux  $\Gamma_r$ computed from the fluctuating density  $(\tilde{n})$  and poloidal electric field  $(\tilde{E}_{\theta})$  by  $\Gamma_r = \langle \tilde{n}\tilde{E}_{\theta} \rangle / B_{\phi}$ , where the brackets denote an ensemble average.  $\tilde{n}$  here was estimated in a usual way from ion saturation current fluctuations and  $\tilde{E}_{\theta}$  from the potential fluctuation difference measured by two poloidally spaced pins of the triple probe. Another probe array with 4 mm radial extension was equipped to detect the floating potential or ion saturation currents  $I_s$ . The local radial electric field  $E_r$ can therefore be estimated from the potential difference measured by two radially separated pins of the fast probe. For the stationary probe system, the probe tips were all arranged to measure either  $\phi_f$  or  $I_s$ . This setup enables the simultaneous investigation of small-scale (on the order of 1 cm) turbulence properties and large-scale (on the order of 10 m) zonal flows in the plasma boundary of TEXTOR. The probe data were digitized at a rate of 500 kHz to provide simultaneous measurements of the edge equilibrium and fluctuation quantities.

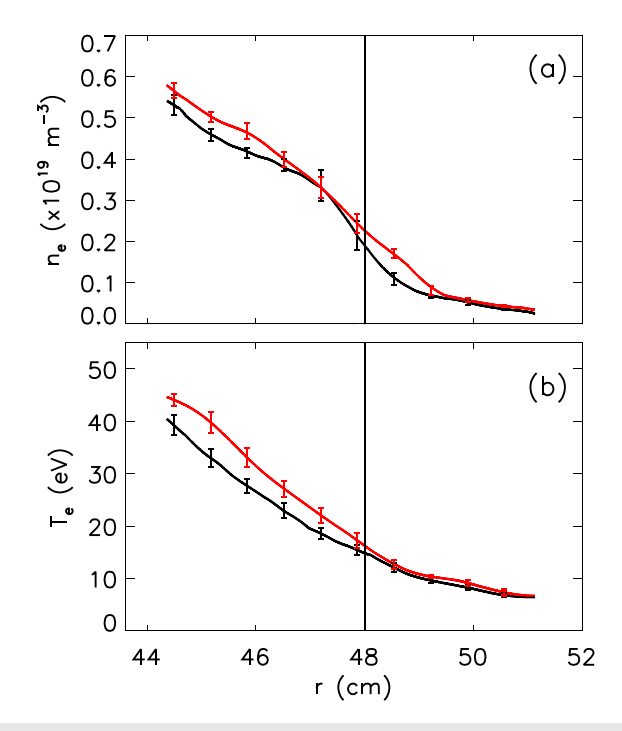
### III. EXPERIMENTAL RESULTS AND DISCUSSION

Figure 1 plots discharge waveforms in a magnetic perturbation experiment. In Figs. 1(a)–1(c), one can see that a dc MP current ( $I_{MP}$ ), ramping from 0 to 7.5 kA and then held constant for about 1 s, was applied in the stationary stage of the discharge. As illustrated in the shaded zones in Figs. 1(b)–1(d), with magnetic perturbation, the edge  $D_{\alpha}$  emission strongly reduces, while the line-averaged density is almost unchanged, implying an improvement of particle confinement. Here, we infer the confinement improvement by evaluating the global particle confinement time  $\tau_p$  from the time derivative of the total electron density  $\frac{dN_e}{dt}$ , which is determined by the ionization rate of neutral



**FIG. 1.** Time evolution of plasma parameters during an m/n=6/2 MP experiment at TEXTOR. (a) Plasma current; (b) dc-MP current; (c) central line-averaged density and  $D_{\alpha}$  emission in front of the ALT limiter at the low-field side along with the horizontal plasma position; (d) raw signal of floating potential measured by the stationary probe at the plasma edge ( $r \approx 46$  cm); (e) radial position of fast reciprocating Langmuir probe arrays; and (f) raw signal of floating potential measured by the fast probe

particles  $(n_e n_0 S_0 V)$  and total loss rate  $(\int \Gamma_{loss} \cdot S = \frac{N_e}{\tau_o})$ , where  $n_e$  and  $n_0$  are the electron density and the neutral density, respectively,  $S_0$  is the ionization rate, and V(S) denotes the total plasma volume (surface area), i.e.,  $\frac{dN_e}{dt}=n_en_0S_0V-\frac{N_e}{\tau_p}.$  On the other hand, the  $D_\alpha$  emission intensity  $I_{D\alpha} \propto n_e n_0 X B$ , where X is the excitation rate and B is the branching ratio of de-excitation. For the same density and temperature,  $\frac{S_0}{XB}$  is nearly constant and  $n_e n_0 S_0 V \propto I_{D\alpha}$ . In our experiment, the total density is almost unchanged ( $\frac{dN_e}{dt} = 0$ ), and we get  $\tau_p = \frac{N_e}{n_e n_0 S_0 V}$  $\propto \frac{N_e}{I_{Du}}$ . Therefore, a reduced  $I_{Du}$  value indicates an enhanced particle confinement time. The question is "what induces a reduction of edge particle transport losses during the magnetic perturbation?" Fig. 1(d) plots the  $\phi_f$  signal measured by the stationary probe at the plasma edge ( $r \approx 46$  cm). It shows a reduction in the fluctuation level during the MP phase. Thus, we have to link the reduced edge transport to the change in turbulence properties. Figure 1(e) draws the time trace of the radial position of the fast reciprocating probe, which moves from the SOL into the plasma edge. In each shot, two plunges were executed for a comparison between the periods before and during the MP. With MP, the mean value of the floating potential is strongly modified, as displayed in the  $\phi_f$  signals in Figs. 1(d) and 1(f) measured by both the stationary and fast probes. This modification is considered to be caused by the ambipolarity constraint along the MP-induced open field lines via which the electrons move faster than massive ions, and hence, the local  $\phi_f$  increases, as observed earlier on Tore Supra, TEXTOR,<sup>24</sup> and MAST.<sup>16</sup> Figure 2 depicts the radial profiles of the



**FIG. 2.** Radial dependence of (a) edge plasma density and (b) electron temperature before (black curves) and during (red curves) the MP measured by the fast probe. The error bars indicate the standard deviation about the mean estimated in similar discharges. The vertical solid line denotes the limiter location.

edge equilibrium density and electron temperature averaged in several analogous discharges measured by the fast probe before (black) and during (red) the MP. It is shown that with MP, both the edge  $n_e$  and  $T_e$  values are slightly enhanced in the plasma edge. As the line-averaged density is almost unchanged, the increase in  $n_e$  is not pronounced.

# A. Impact of magnetic perturbation on turbulent transport in different perturbation zones at the plasma boundary

For studying the influence of the magnetic perturbation on plasma parameters, it is important to know the magnetic penetration depth and the local modification of the magnetic topology by the MP so that one can explore how turbulence and turbulent transport are affected in different penetration zones. During the MP operation, the magnetic perturbation leads to a chaotic behavior of the field lines in the plasma boundary. In general, the stochastic field lines can be sorted into two distinct regions, i.e., the "ergodic zone" (EZ) with a longer field line connection length ( $L_c$  > the Kolmogorov decay length, a statistical measure of the e-folding length for the exponential separation of neighboring field lines) and the "laminar zone" (LZ) with shorter  $L_c$ . In practice, the EZ and LZ are distinguished by  $L_c \approx 3-4$  poloidal turns of the torus, as predicted by calculations.<sup>28</sup> In this investigation, we have calculated the connection lengths of field lines using the ATLAS code<sup>29</sup> at the location where the probe measurements were executed during the MP. The radial variation of  $L_c$  is plotted in Fig. 3(a) together with the radial profiles of  $E_r$  shear  $(E'_r)$ , fluctuationinduced particle flux  $\Gamma_r$ , and the poloidal turbulence correlation length  $(l_{\theta})$  measured in the EZ, LZ, and SOL regions before (black) and during (red) the MP. Here,  $l_{\theta}$  is computed by the inverse of the  $k_{\theta}$  spectrum width of potential fluctuations detected by two poloidally spaced probes.<sup>30</sup> Figure 3(b) shows that with MP, the absolute value of  $E'_r$  is reduced in all three regions. In the SOL (48 cm < r < 50 cm) where the stochastization is weak,  $\Gamma_r$  slightly increases, and it appears to react to locally decreased  $E'_r$ . In the EZ,  $\Gamma_r$  is strongly reduced, in line with the reduction of the edge transport and improved particle confinement. The drop of  $\Gamma_r$  in the ergodic zone cannot be attributed to the locally reduced  $E'_r$ . As the local  $l_\theta$  in the EZ and LZ decreases during the MP phase [see Fig. 3(d)], it turns to be the destructive role by the MP itself on turbulence eddies, which leads to a drop of turbulent flux in the stochastic region. Similar results for the MP suppression on large turbulence structures have also been observed elsewhere, 8,9,16,24 in agreement with theoretical simulations.<sup>31</sup> It is, however, noticed that in the simulation of microturbulence in the DIII-D H-mode pedestal region, the resonant magnetic perturbation does not significantly affect the electrostatic mode structure. 32

## B. Impact of magnetic perturbation on multi-scale turbulence and turbulent flux in the ergodic zone

In order to explore the impact of the magnetic perturbation on multi-scale turbulence components and on turbulence-driven transport, we have computed the frequency spectra of various fluctuation quantities and their contributions to the fluctuation-induced particle flux in the EZ area before and during the MP. Figure 4 depicts the spectral components of the turbulent particle flux  $\Gamma_r(f) = \frac{\langle \tilde{n}(f)\tilde{E}_{\theta}(f)\rangle}{B_{\phi}} = \frac{k_{\theta}(f)|P_{n\phi}(f)|\times\sin[z_{n\phi}(f)]}{B_{\phi}} = \frac{k_{\theta}(f)|\tilde{n}^{ms}(f)\tilde{\phi}^{rms}(f)\gamma_{n\phi}(f)\times\sin[z_{n\phi}(f)]}{B_{\phi}}$ , where  $\tilde{n}^{rms}$  and

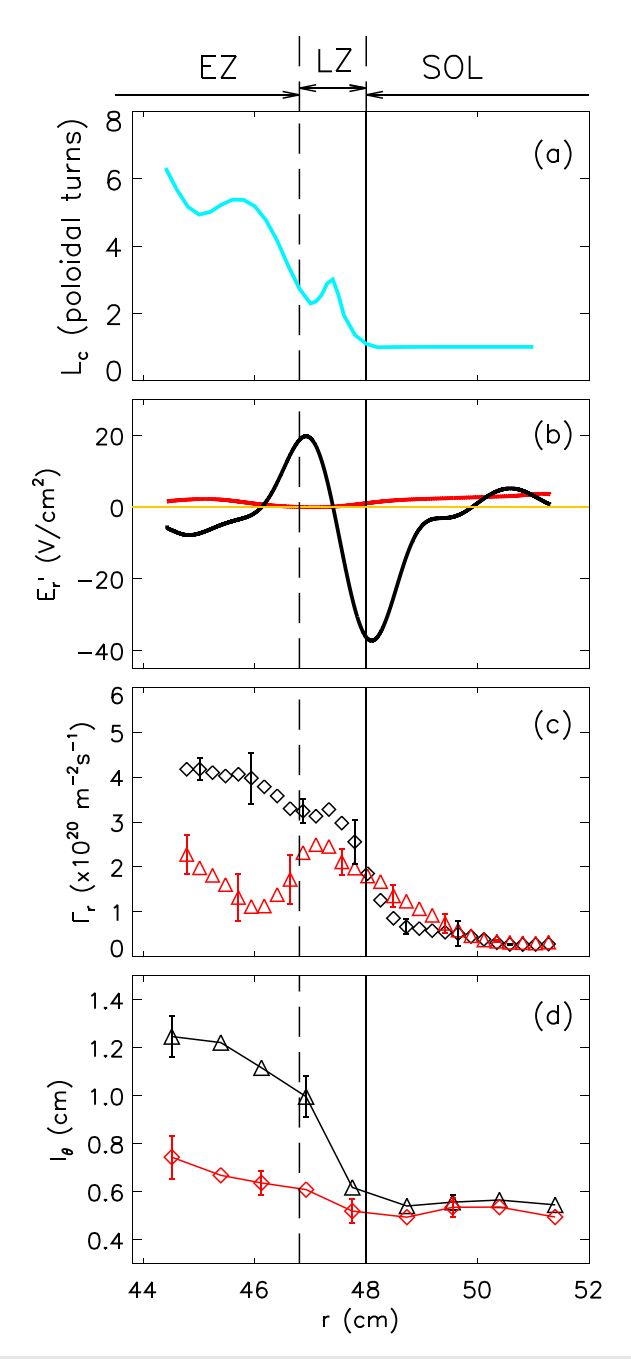


**FIG. 3.** Radial profiles of (a) the calculated field line connection length (normalized by the poloidal turn flux tube), (b)  $E_r$  shear, (c) fluctuation-driven particle flux, and (d) the poloidal correlation length detected by the fast probe before (black curves/symbols) and during (red curves/symbols) the MP. The vertical solid line denotes the limiter position. The vertical dashed line roughly separates the ergodic zone (EZ, left side) and the laminar zone (LZ, right side).

 $\tilde{\phi}^{rms}$  denote the root mean square (rms) level of density and potential fluctuations,  $\gamma_{n\phi}$  is the coherence between  $\tilde{n}$  and  $\tilde{\phi}$ , and  $\alpha_{n\phi}$  is the phase difference between  $\tilde{n}$  and  $\tilde{\phi}$ . In the Ohmic phase before the MP (black curves), the turbulence spectra roughly contain two major parts.

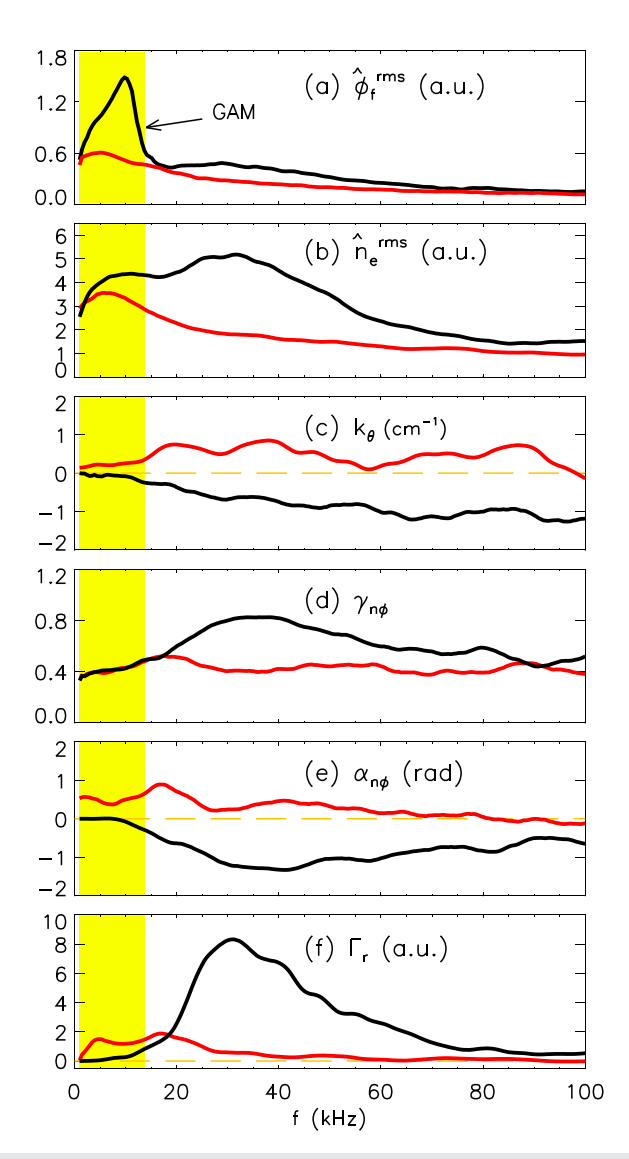


**FIG. 4.** Comparison of turbulent particle flux and its spectral components measured by the fast probe at  $r\approx45.8$  cm before (black curves, without MP) and during (red curves, with MP) the edge transport reduction (# 111625). (a) The root mean square (rms) level of potential fluctuations, (b) the rms level of density fluctuations, (c) the poloidal wavenumber, (d) the coherence between density and potential fluctuations, (e) the phase difference between density and potential fluctuations, and (f) turbulent particle flux as a function of frequency.

In the low-frequency range ( $f<15\,\mathrm{kHz}$ ),  $\tilde{\phi}^{rms}(f)$  exhibits a prominent peak around  $f\approx10\,\mathrm{kHz}$ , as shown in Fig. 4(a). It has been found that this peaked component is attributed to the large-scale geodesic acoustic mode (GAM) zonal flows, which has a narrow radial extent and the poloidal/toroidal mode number m/n=0/0 in potential fluctuations. The detailed properties of this GAM have been investigated and documented in Refs. 33 and 34. In the higher frequency range ( $f>15\,\mathrm{kHz}$ ), the small-scale drift-wave turbulence contributes to the potential and density fluctuation power. As shown in Fig. 4(f), before MP, the turbulent particle flux  $\Gamma_r$  is mainly driven by small-scale

ambient turbulence, while the GAM zonal flow makes little contribution to  $\Gamma_r$  since the poloidal wavenumber  $k_{\theta}(f)$  of the GAM is close to zero in the low frequency range. In the period of confinement improved with the MP, all the spectral components of  $\Gamma_r(f)$  are changed significantly. First, the magnetic perturbation induces an overall reduction in potential and density fluctuation amplitudes,  $\tilde{n}^{rms}(f)$  and  $\tilde{\phi}^{rms}(f)$ , implying suppression by MP on both GAM zonal flows and ambient turbulence. The destructive role by the MP on the large-scale GAMs has been observed earlier in TEXTOR<sup>13</sup> and in other tokamaks as well. 18,19 The absence of GAM during the MP leads to development of nonzero  $k_{\theta}$  in the low frequency fluctuations [see the red curve in Fig. 4(c)], and meanwhile, we observed an increase in  $\Gamma_r$  in the low frequency range. It is interesting to note that in the present discharge, the MP induces simultaneous changes in the sign of  $\alpha_{n\phi}(f)$  ( $|\alpha_{n\phi}| < 90^{\circ}$ ) and  $k_{\theta}(f)$  so that  $\Gamma_r$  remains in the radially outward direction. During MP, the coherence  $\gamma_{n\phi}$  of ambient turbulence decreases, indicating the reduction of cross-power between density and potential fluctuations in terms of the rms value of the fluctuations. The above results reveal that for the present experiments, (i) the application of magnetic perturbation, in general, imposes a suppression role on multi-scale fluctuation components, including largescale GAM zonal flows and small-scale drift-wave turbulence; and (ii) with MP, the edge transport reduction (or confinement improvement) arises primarily from strong reduction of small-scale ambient turbulence, whereas in the low frequency range, the application of MP stirs a small enhancement to turbulent transport owing to suppression of GAMs.

### C. Dynamics of nonlinear interaction and energy transfer between GAM zonal flows and ambient turbulence (AT) across transport reduction induced by the MP

In the physics of zonal flows, it is well known that GAM zonal flows usually coexist with drift-wave ambient edge turbulence (AT) and their dynamic interaction can be characterized from two different manifestations, which are not mutually exclusive.<sup>35</sup> One is that the GAM extracts energy from AT via nonlinear coupling, while the other is the reduction of AT by the time-varying  $E \times B$  shear decorrelation.<sup>36</sup> For the second effects, we have estimated the  $E \times B$  shear rate by GAM zonal flows and found that it is nearly one order lower than the decorrelation rate of AT. Thus, in our case, the shearing effects by GAM on AT are not significant enough to cause the L-H transition. Therefore, in this study, we focus on the first aspect of interaction dynamics between GAM and AT, i.e., the nonlinear energy transfer between GAM and AT. In our experiment, the MP suppresses both GAM zonal flows and AT and eventually triggers a reduction of edge transport (or improved confinement). Therefore, it is essential to survey the dynamics of the nonlinear coupling between GAM and AT during the process that both are gradually reduced with increasing MP magnitude. To this end, we first investigate the self-regulation process of the GAM for the drift-wave turbulence in the Ohmic discharge phase without employing the MP. The results are illustrated in Fig. 5, in which the time traces of  $\phi_f$ ,  $\tilde{E}_r$ , and  $\tilde{I}_s$  were detected by the fast probe array in the ergodic zone ( $r \approx 46$  cm). Whereas both  $\phi_f$  and  $\tilde{E}_r$ signals are oscillating at the GAM frequency (see red curves filtered in 7–12 kHz),  $\tilde{I}_s$  exhibits broad-band features. Here,  $\tilde{I}_s$  can be treated as a proxy of ambient density fluctuations. In Fig. 5(c), the envelope of  $I_s$ 

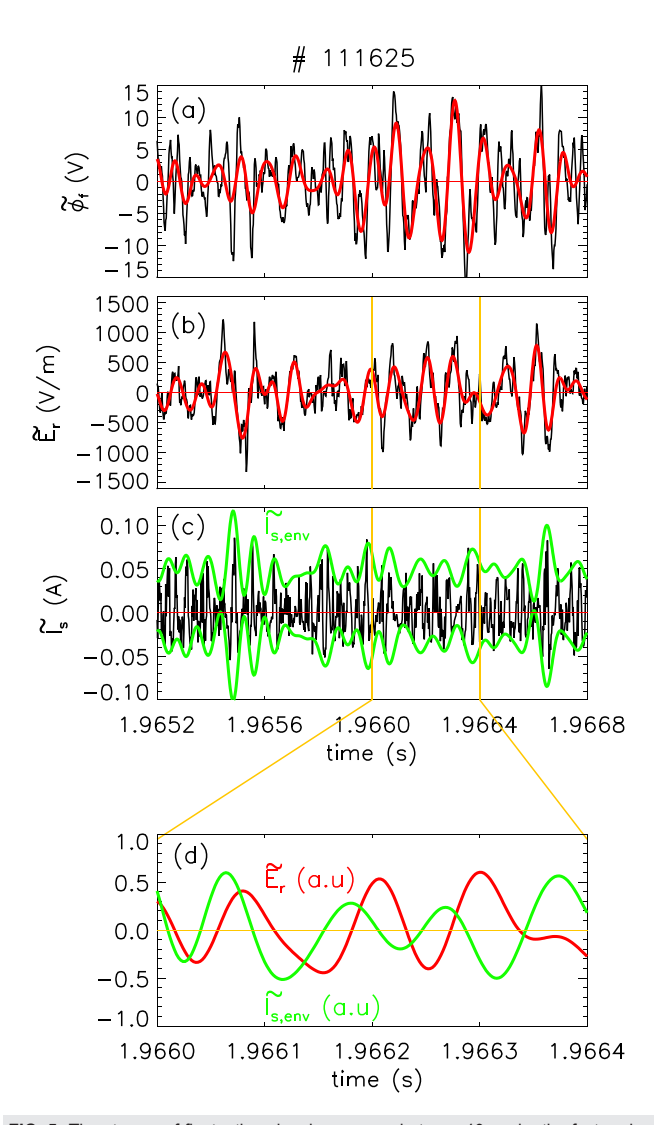


**FIG. 5.** Time traces of fluctuation signals measured at  $r\approx 46$  cm by the fast probe before MP. (a) Floating potential  $\tilde{\phi}_f$ , (b) radial electric field  $\tilde{E}_r$ , and (c) ion situation current  $\tilde{I}_s$  and its envelope  $\tilde{I}_{s,env}$  depicted by the green curve. The red curves in (a) and (b) indicate the GAM oscillation filtered from the raw signals. The lower zoomed panel compares the temporal evolution of  $\tilde{E}_r$  (red curve) and the envelope of  $\tilde{I}_s$  (green curve).

 $(\tilde{I}_{s,env})$  is calculated via the Hilbert transform and depicted by green curves. It can be clearly seen that the AT  $(\tilde{I}_s)$  is modulated by the frequency of GAM zonal flows. Similar phenomena have been observed in JFT-2M tokamak.<sup>37</sup> Figure 5(d) compares the temporal evolutions of  $\tilde{E}_r$  (filtered around the GAM frequency) and  $\tilde{I}_{s,env}$ .  $\tilde{E}_r$  oscillation lags the  $\tilde{I}_{s,env}$  variation by about  $\pi/2$ , consistent with the predator-prey dynamics, i.e., the GAM zonal flows act as a predator and AT is a prey. Such kinds of predator-prey interaction between another type low-frequency  $\tilde{E}_r \times B$  zonal flow and the ambient turbulence leading to the L–H transition have been described in Ref. 38 and experimentally identified during the period of the limit cycle oscillation prior to the L–H transition.  $^{39,40}$  To verify the above results, we have calculated

the cross correlation function (CCF) from the  $\tilde{E}_r$ ,  $\tilde{\phi}_f$ , and  $\tilde{I}_{s,env}$  signals and averaged the CCF values over a number of ensembles. The results are depicted in Fig. 6. In Fig. 6(a), the CCF between  $E_r$  and  $I_{s,env}$  and the CCF between  $\widetilde{\phi}_f$  and  $\widetilde{I}_{s,env}$  signals computed from the fast probe data in the EZ region are shown by the black and blue curves, respectively. The CCF  $(\tilde{E}_r - \tilde{I}_{s,env}) = 0$  at the zero time lag affirms the  $\pi/2$ phase difference between the predator  $(\tilde{E}_r)$  and prey  $(\tilde{I}_{s,env})$  oscillations. Because  $\tilde{E}_r = -ik_r\phi_f$ , the variation of  $\phi_f$  lags  $\tilde{E}_r$  by  $\pi/2$ . Thus, the phase delay between CCF ( $\phi_f$ - $\tilde{I}_{s,env}$ ) and CCF ( $\tilde{E}_r$ - $\tilde{I}_{s,env}$ ) is nearly a quarter of the period (T/4). Similarly, the local CCF  $(\phi_f - \tilde{I}_{s,env})$  measured by the stationary probe pins at approximately the same radial position but a distant toroidal location of the torus has been calculated and is plotted in Fig. 6(b). It shows analogous variations to the CCF  $(\phi_f - I_{s,env})$  detected by the fast probes. As the value of CCF  $(\phi_f - I_{s,env})$ depends on the strength of the GAM zonal flows and its nonlinear coupling with the AT, we may use its peak-peak value (magnitude) as a rough measure to quantify the degree of the nonlinear interaction between the GAM and the AT.

The influence of the MP on the dynamics of the nonlinear coupling and energy transfer between the GAM zonal flows and AT is further inspected in the ramp-up phase of the perturbation current ( $I_{MP}$ ), during which a reduced edge transport (or improved confinement) is excited. Figure 7 plots time histories of  $I_{MP}$  (increasing from 0 to 7.5 kA) and related fluctuation quantities measured by the stationary probe located at a fixed radial position in the EZ area across a transition to an improved confinement. To obtain better statistics, the

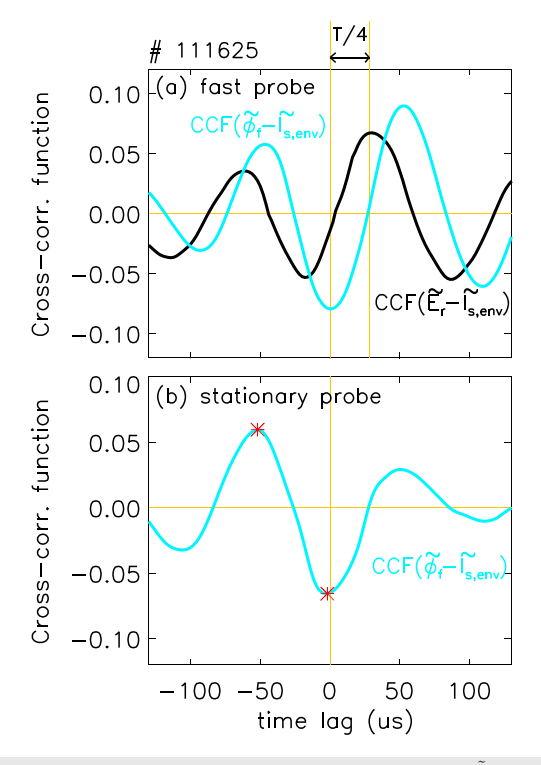


**FIG. 6.** (a) Cross-correlation function (CCF) between fluctuating  $\tilde{E}_r$  and the  $I_s$  envelope (black curve) and  $\bar{\phi}_f$  and the  $I_s$  envelope (blue curve) at  $r\approx 46$  cm measured by the fast probe before MP. (b) CCF between fluctuating  $\bar{\phi}_f$  and the  $\bar{I}_s$  envelope measured by the stationary probe ( $r\approx 46$  cm) before MP.

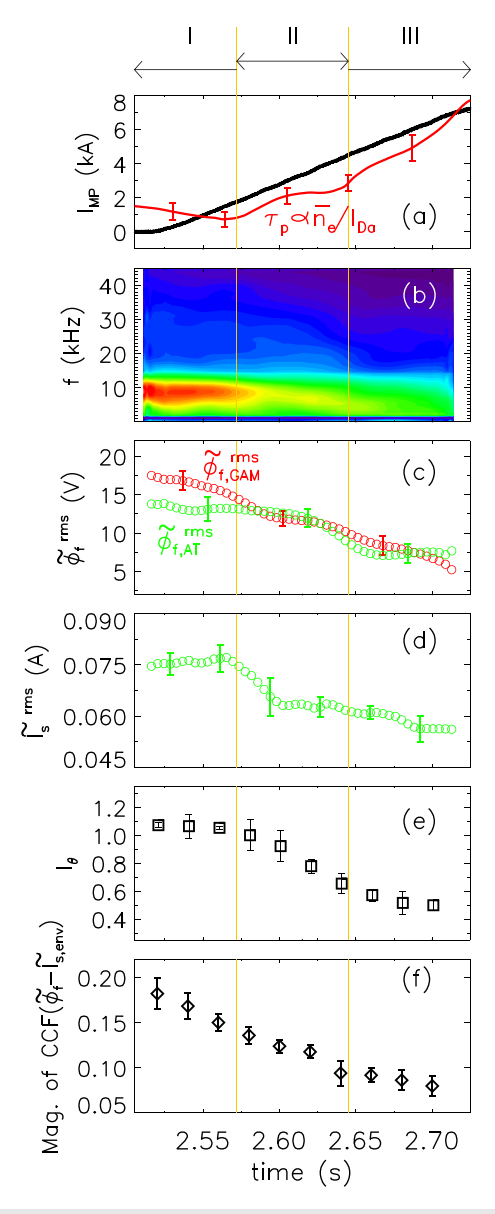


**FIG. 7.** Time evolutions of (a) MP current and the ratio of  $\bar{n}_e/I_{D_{\rm Z}}(\propto \tau_p)$ ; (b) contour-plot of spectra of  $\phi_f$  fluctuations; (c) rms level of GAM zonal flows  $(\tilde{\phi}_{f,GAM}^{rms})$  and ambient turbulence  $(\tilde{\phi}_{f,AT}^{rms})$  in potential fluctuations; (d) rms level of density fluctuations  $(\tilde{I}_{s}^{rms})$ ; (e) poloidal correlation length; and (f) magnitude of the cross correlation between fluctuating  $\tilde{\phi}_f$  and  $\tilde{I}_{s,env}$  measured by the stationary probe  $(r\approx 46$  cm). The results were averaged over a few similar discharges. The error bars indicate the standard deviation about the mean estimated in these shots.

results in Fig. 7 have been averaged over several similar discharges. In Fig. 7(a), we added the time trace of the ratio  $\bar{n}_e/I_{D\alpha}$  as an indication of the change in the particle confinement time  $\{\tau_p \propto \bar{n}_e/I_{D\alpha}$ , while the density is stable [see Fig. 1(c)]}. One can see that the increase in  $\tau_p$  occurs when the MP current rises to  $\sim 2\,\mathrm{kA}$ . Figure 7(b) displays the contour-plot of the potential fluctuation  $\bar{\phi}_f$  spectra. For separating the GAM and AT components, Fig. 7(c) plots their rms levels estimated

from the raw  $\phi_f$  signal filtered in the frequency range of (1–20) kHz and (20-100) kHz, respectively. As background turbulence, the rms level of  $\tilde{I}_s$  is drawn in Fig. 7(d). The spatial structure of the turbulence eddies is evaluated by calculating the poloidal correlation length ( $l_{\theta}$ ) of  $ilde{\phi}_f$  measured by two poloidally spaced pins at the stationary probe. It should be pointed out that the contribution from the GAM zonal flows to the measured  $l_{\theta}$  has been excluded since the GAM has a poloidal homogeneous structure (m=0) in potential fluctuations. Hence, the time evolution of  $l_{\theta}$  in Fig. 7(e) only reflects variations of small-scale AT structures affected by the magnetic perturbation. In Fig. 7(f), the magnitude of the  $CCF(\phi_f - \tilde{I}_{s,env})$  detected by the stationary probe system is depicted, which is used to assess the nonlinear coupling degree between GAM and AT. It is found that across the whole MP ramp-up period, the dynamic processes of GAM and AT variations and their nonlinear interplay can be generally divided into three stages, as marked in the figure. In phase-I, at small MP currents ( $I_{MP}$  < 2 kA),  $ilde{\phi}_{f,AT}^{\it rms}, ilde{l}_s^{\it rms}$ , and  $ilde{l}_{ heta}$  are nearly unchanged, while  $ilde{\phi}_{f,GAM}^{\it rms}$  decreases rapidly with increasing  $I_{MP}$ . This means that the large-scale GAM is more sensitive than the micro-scale AT in response to a small magnetic perturbation. As a consequence, the nonlinear energy transfer between the GAM and AT also reduces gradually with increasing  $I_{MP}$ , as shown in Fig. 7(f). In this phase, the plasma confinement is slightly deteriorated due to the reduction of the GAM [see  $\tau_p \propto \bar{n}_e/I_{D\alpha}$  in Fig. 7(a)]. In the second phase (2 kA <  $I_{MP}$  < 4.5 kA), all  $\phi_{f,AT}^{...}$ ,  $\phi_{f,GAM}^{...}$ ,  $\tilde{I}_{s}^{rms}$ ,  $l_{\theta}$ , and  $\text{CCF}(\tilde{\phi}_{f}-\tilde{I}_{s,env})$  quantities decrease gradually with increasing perturbation current, indicating that both large-scale GAM and small-scale AT are strongly reduced by the MP, and meanwhile, their nonlinear interaction and energy transfer drop further. Note that  $\tau_p$  starts to increase at the beginning of this phase, which suggests that (i) the edge transport reduction is induced primarily due to repression of small-scale ambient turbulence and (ii) for triggering an edge transport reduction (or confinement improvement), a threshold MP strength is needed for suppressing the AT. In phase-III  $(I_{MP} > 4.5 \text{ kA})$ , with a further increase in  $I_{MP}$ , both GAM and AT are strongly suppressed, and the GAM zonal flows vanish eventually. Therefore,  $\tau_p$  increases continuously in this phase. The above results show that during the entire MP ramp-up period, the GAM zonal flows and their nonlinear interaction with background turbulence decrease incessantly. The decrease in edge transport does not occur until the micro-scale turbulence starts to be suppressed by the MP when the perturbation current reaches a certain threshold value.

It should be noted that in the MP experiments, the magnetic perturbation at the plasma boundary may alter the magnetic topology and even generate magnetic islands, depending on the penetration strength. In the present m/n=6/2 MP operation, small island chains have been observed although large islands were not yet excited. The local change of the sheared flows around the island boundary may also be one possible mechanism to cause particle confinement changes. The role of magnetic islands along with other mechanisms in affecting plasma transport and confinement properties will be investigated in the future.

### **IV. CONCLUSION**

In conclusion, the impact of edge magnetic perturbation on multi-scale turbulence and turbulent transport has been studied in detail in a peculiar improved Ohmic confinement regime at the TEXTOR tokamak. The results show that the magnetic perturbation generally imposes a suppression effect on both the large-scale GAM zonal flows and micro-scale drift-wave turbulence. At small MP currents, the repression of GAM zonal flows is more sensitive than smallscale ambient turbulence. With increasing MP strength, an edge transport reduction (or confinement improvement) can be triggered due to mainly the destructive role of the MP on small-scale turbulence eddies, although the suppression of GAMs induces a small enhancement in turbulent transport in the low frequency range. During the entire MP ramp-up phase, the GAM zonal flows and their nonlinear interaction with ambient turbulence decrease incessantly with increasing MP current. The edge transport reduction (or confinement improvement) occurs only after micro-scale turbulence starts to be suppressed by the MP when the MP magnitude reaches a certain threshold value. The results may provide additional implication for the influence of the edge magnetic perturbation on multi-scale turbulence dynamics and turbulent transport at the boundary of fusion devices.

### **ACKNOWLEDGMENTS**

The authors are very grateful to the TEXTOR team for their operational assistance in the experiments. This work was partially supported by the National Natural Science Foundation of China through Grant Nos. 11820101004, 11575057, and 11705051 and partially supported by the National Key R&D Program of China (Grant Nos. 2017YFE0301802 and 2017YFE0301100).

#### DATA AVAILABILITY

The data that support the findings of this study are available from the corresponding author upon reasonable request.

### **REFERENCES**

- <sup>1</sup>T. E. Evans, R. A. Moyer, P. R. Thomas, J. G. Watkins, T. H. Osborne, J. A. Boedo, E. J. Doyle, M. E. Fenstermacher, K. H. Finken, R. J. Groebner *et al.*, Phys. Rev. Lett. **92**, 235003 (2004).
- <sup>2</sup>Y. Liang, H. R. Koslowski, P. R. Thomas, E. Nardon, B. Alper, P. Andrew, Y. Andrew, G. Arnoux, Y. Baranov, M. Bećoulet et al., Phys. Rev. Lett. 98, 265004 (2007).
- <sup>3</sup>W. Suttrop, T. Eich, J. C. Fuchs, S. Günter, A. Janzer, A. Herrmann, A. Kallenbach, P. T. Lang, T. Lunt, M. Maraschek *et al.*, Phys. Rev. Lett. **106**, 225004 (2011).
- <sup>4</sup>Y. In, J.-K. Park, Y. M. Jeon, J. Kim, G. Y. Park, J.-W. Ahn, A. Loarte, W. H. Ko, H. H. Lee, J. W. Yoo *et al.*, Nucl. Fusion **57**, 116054 (2017).
- <sup>5</sup>T. C. Hender, R. Fitzpatrick, A. W. Morris, P. G. Carolan, R. D. Durst, T. Edlington, J. Ferreira, S. J. Fielding, P. S. Haynes, J. Hugill *et al.*, Nucl. Fusion **32**, 2091 (1992).
- <sup>6</sup>Y. Q. Liu and A. Bondeson, Phys. Rev. Lett. **84**, 907 (2000).
- <sup>7</sup>S. A. Sabbagh, J. W. Berkery, R. E. Bell, J. M. Bialek, S. P. Gerhardt, J. E. Menard, R. Betti, D. A. Gates, B. Hu, O. N. Katsuro-Hopkins *et al.*, Nucl. Fusion 50, 025020 (2010).
- <sup>8</sup>J. Payan, X. Garbet, J. H. Chatenet, F. Clairet, C. D. Michelis, P. Devynck, P. Ghendrih, C. Gil, A. Grosman, R. Guirlet *et al.*, Nucl. Fusion **35**, 1357 (1995).
- <sup>9</sup>P. Devynck, X. Garbet, P. Ghendrih, J. Gunn, C. Honore, B. Pégourié, G. Antar, A. Azeroual, P. Beyer, C. Boucher et al., Nucl. Fusion 42, 697 (2002).
- <sup>10</sup>R. A. Moyer, T. E. Evans, T. H. Osborne, P. R. Thomas, M. Becoulet, J. Harris, K.-H. Finken, J. A. Boedo, E. J. Doyle, M. E. Fenstermacher et al., Phys. Plasmas 12, 056119 (2005).
- <sup>11</sup>Y. Xu, R. R. Weynants, S. Jachmich, M. Van Schoor, M. Vergote, P. Peleman, M. W. Jakubowski, M. Mitri, D. Reiser, B. Unterberg et al., Phys. Rev. Lett. 97, 165003 (2006).
- <sup>12</sup>Y. Xu, R. R. Weynants, M. Van Schoor, M. Vergote, S. Jachmich, M. W. Jakubowski, M. Mitri, O. Schmitz, B. Unterberg, P. Beyer *et al.*, Nucl. Fusion 49, 035005 (2009).

- <sup>13</sup>Y. Xu, D. Carralero, C. Hidalgo, S. Jachmich, P. Manz, E. Martines, B. van Milligen, M. A. Pedrosa, M. Ramisch, I. Shesterikov *et al.*, Nucl. Fusion 51, 063020 (2011).
- <sup>14</sup>A. Krämer-Flecken, Y. Xu, S. Soldatov, M. Jakubowski, Y. Liang, D. Reiser, and O. Schmitz, J. Plasma Fusion Res., Ser. 8, 44 (2009).
- <sup>15</sup>J. W. Coenen, O. Schmitz, B. Unterberg, M. Clever, M. A. Jakubowski, U. Samm, B. Schweer, H. Stoschus, and M. Tokar, Nucl. Fusion 51, 063030 (2011).
- <sup>16</sup>P. Tamain, A. Kirk, E. Nardon, B. Dudson, and B. Hnat, Plasma Phys. Controlled Fusion 52, 075017 (2010).
- <sup>17</sup>Y. Sun, Y. Liang, H. R. Koslowski, S. Jachmich, A. Alfier, O. Asunta, G. Corrigan, C. Giroud, M. P. Gryaznevich, D. Harting *et al.*, Plasma Phys. Controlled Fusion 52, 105007 (2010).
- <sup>18</sup>J. R. Robinson, B. Hnat, A. Thyagaraja, K. G. McClements, P. J. Knight, and A. Kirk, Plasma Phys. Controlled Fusion 54, 105007 (2012).
- <sup>19</sup>G. D. Conway, S. Fietz, H. W. Müller, T. Lunt, P. Simon, W. Suttrop, M. Maraschek, T. Happel, and E. Viezzer, Plasma Phys. Controlled Fusion 57, 014035 (2015).
- <sup>20</sup>S. Mordijck, T. L. Rhodes, L. Zeng, E. J. Doyle, L. Schmitz, C. Chrystal, T. J. Strait, and R. A. Moyer, Plasma Phys. Controlled Fusion 58, 014003 (2016).
- <sup>21</sup>M. Jiang, Y. Xu, W. L. Zhong, D. Li, Z. Huang, Z. J. Yang, Z. B. Shi, N. C. Wang, Z. F. Cheng, Z. C. Yang et al., Nucl. Fusion 59, 046003 (2019).
- <sup>22</sup>K. H. Finken, S. S. Abdullaev, M. W. Jakubowski, M. F. M. de Bock, S. Bozhenkov, C. Busch, M. von Hellermann, R. Jaspers, Y. Kikuchi, A. Krämer-Flecken et al., Phys. Rev. Lett. 98, 065001 (2007).
- <sup>23</sup>K. H. Finken, S. S. Abdullaev, W. Biel, M. F. M. de Bock, C. Busch, E. Farshi, M. von Hellermann, G. M. D. Hogeweij, M. Jakubowski, R. Jaspers *et al.*, Plasma Phys. Controlled Fusion 46, B143 (2004).
- <sup>24</sup>Y. Xu, M. Van Schoor, R. R. Weynants, S. Jachmich, M. Vergote, M. W. Jakubowski, P. Beyer, M. Mitri, B. Schweer, D. Reiser *et al.*, Nucl. Fusion 47, 1696 (2007).

- <sup>25</sup>S. Chen and T. Sekiguchi, J. Appl. Phys. **36**, 2363 (1965).
- <sup>26</sup>P. C. Stangeby and G. M. McCracken, Nucl. Fusion **30**, 1225 (1990).
- <sup>27</sup>J. Wesson, *Tokamaks*, 4th ed. (Oxford University Press, 2011).
- <sup>28</sup>M. W. Jakubowski, O. Schmitz, S. S. Abdullaev, S. Brezinsek, K. H. Finken, A. Krämer-Flecken, M. Lehnen, U. Samm, K. H. Spatschek, B. Unterberg et al., Phys. Rev. Lett. 96, 035004 (2006).
- <sup>29</sup>M. W. Jakubowski, S. S. Abdullaev, and K. H. Finken, Nucl. Fusion 44, S1 (2004).
- 30 J. M. Beall, Y. C. Kim, and E. J. Powers, J. Appl. Phys. 53, 3933 (1982).
- <sup>31</sup>D. Reiser, Phys. Plasmas 14, 082314 (2007).
- <sup>32</sup>I. Holod, Z. Lin, S. Taimourzadeh, R. Nazikian, D. Spong, and A. Wingen, Nucl. Fusion 57, 016005 (2017).
- <sup>33</sup>Y. Xu, I. Shesterikov, M. Van Schoor, M. Vergote, R. R. Weynants, A. Krämer-Flecken, S. Zoletnik, S. Soldatov, D. Reiser, K. Hallatschek *et al.*, Plasma Phys. Controlled Fusion 53, 095015 (2011).
- <sup>34</sup>A. Krämer-Flecken, S. Soldatov, H. R. Koslowski, and O. Zimmermann, Phys. Rev. Lett. 97, 045006 (2006).
- 35P. H. Diamond, S.-I. Itoh, K. Itoh, and T. S. Hahm, Plasma Phys. Controlled Fusion 47, R35 (2005).
- <sup>36</sup>T. S. Hahm, M. A. Beer, Z. Lin, G. W. Hammett, W. W. Lee, and W. M. Tang, Phys. Plasmas 6, 922 (1999).
- <sup>37</sup>T. Ido, Y. Miura, K. Kamiya, Y. Hamada, K. Hoshino, A. Fujisawa, K. Itoh, S.-I. Itoh, A. Nishizawa, H. Ogawa et al., Plasma Phys. Controlled Fusion 48, S41–S50 (2006).
- <sup>38</sup>E. J. Kim and P. H. Diamond, *Phys. Rev. Lett.* **90**, 185006 (2003).
- <sup>39</sup>L. Schmitz, L. Zeng, T. L. Rhodes, J. C. Hillesheim, E. J. Doyle, R. J. Groebner, W. A. Peebles, K. H. Burrell, and G. Wang, Phys. Rev. Lett. 108, 155002 (2012).
- <sup>40</sup>J. Cheng, J. Q. Dong, K. Itoh, L. W. Yan, M. Xu, K. J. Zhao, W. Y. Hong, Z. H. Huang, X. Q. Ji, W. L. Zhong *et al.*, Phys. Rev. Lett. **110**, 265002 (2013).